Atmospheric Environment 195 (2018) 149–158

Contents lists available at ScienceDirect

Atmospheric Environment

journal homepage: www.elsevier.com/locate/atmosenv

Estimating PM_1 concentrations from MODIS over Yangtze River Delta of China during 2014–2017

Kai Qin[a], Jiaheng Zou[a], Jianping Guo[b,*], Meng Lu[c], Muhammad Bilal[d], Kefei Zhang[a], Fangfang Ma[a], Yishu Zhang[a]

[a] School of Environment Science and Spatial Informatics, China University of Mining and Technology, Xuzhou, China
[b] State Key Laboratory of Severe Weather, Chinese Academy of Meteorological Sciences, Beijing, China
[c] Department of Physical Geography, Utrecht University, Utrecht, Netherlands
[d] School of Marine Sciences, Nanjing University of Information Science & Technology, Nanjing, China

ARTICLE INFO

Keywords:
PM_1
Aerosol optical depth
Satellite
China
Yangtze river delta

ABSTRACT

Compared to the space-borne estimation of $PM_{2.5}$ (particulate matter with aerodynamic diameter ≤2.5 μm), the investigation of PM_1 (≤1 μm) remains less intensive and thus unclear. Here we estimated four years (2014–2017) of ground-level PM_1 concentrations from MODIS aerosol optical depth (AOD) in attempt to gain a better understanding of much finer particles. The Yangtze River Delta (YRD) region, with a relatively dense ground-based PM_1 station network, was selected as the study area. The geographically and temporally weighted regression (GTWR) model simultaneously accounting for spatial and temporal variability existing within various predictors was constructed. Validation of satellite-estimated PM_1 against ground-measured PM_1 yields a high consistence, significant improvement over previous work (R^2 = 0.74 VS 0.59, RMSE = 13.02 μg/m^3 VS 22.5 μg/m^3). This suggests the PM_1 estimates from GTWR model are reliable and robust enough to obtain large-scale fine particle contents. The population exposure of air pollution in the YRD region, therefore, has been analyzed by calculating population-weighted mean PM_1 concentrations, which reaches as high as 37.22 μg/m^3. Further analysis indicates that near half the people live in locations with high-level PM_1 concentration (> 35 μg/m^3), which has profounding implication for improving our understanding of human exposure to fine aerosol particles.

1. Introduction

China is suffering from serious air pollution (Che et al., 2014; Guo et al., 2016b; Chen et al., 2017a; Tong et al., 2018a, 2018b; 2018c; Luo et al., 2018; Liu et al., 2018a; Yang et al., 2018), which is dominated with aerosol particles that adversely affect human health (Gu and Yim, 2016; Cohen et al., 2017; Li et al., 2017; Ho et al., 2017; Gu et al., 2018). PM_1 (particulate matter with aerodynamic diameter≤1 μm), a major component of $PM_{2.5}$ (≤2.5 μm), is more harmful than $PM_{2.5}$ due to its smaller particle size that makes it easily reach deeper into the respiratory system (Agudelo-Castañeda et al., 2017; Chen et al., 2017b).

Due to its large spatial coverage, satellite-retrieved aerosol optical depth (AOD) has been widely used to obtain the large-scale variabilities of ground-level aerosol particles (Wang and Christopher, 2003; Van Donkelaar et al., 2006; Gupta et al., 2006, 2007; Paciorek et al., 2008; Martin, 2008; Liu et al., 2005, 2007, 2009; Wu et al., 2012; Just et al., 2015; Xu et al., 2016; Guo et al., 2017, 2017), most of which are limited to $PM_{2.5}$ or PM_{10}. The methods used to estimate PM from space based on the AOD-PM relationships include semi-empirical methods based on *a priori* knowledge (e.g., Tian et al., 2010; Wang et al., 2010; Lin et al., 2016), simulation-based methods using chemical transport models (e.g., Van Donkelaar et al., 2010; Geng et al., 2015), and statistical methods that require sufficient ground station measurements (e.g., Lee et al., 2011; Kloog et al., 2012; Beckerman et al., 2013; Hu et al., 2014; Liu et al., 2018).

In particular, the estimates of $PM_{2.5}$ in China from space are increasingly relying on statistical methods, considering the huge amount of $PM_{2.5}$ observations (about 1500 stations) being released for public access by Chinese government since 2013. These statistical methods include the geographically weighted regression model (Song et al., 2014; Ma et al., 2014; You et al., 2016; Zou et al., 2016a), the geographically and temporally weighted regression (GTWR) model (Bai et al., 2016), the linear mixed effect model (Ma et al., 2016a,b; Wang et al., 2012), the generalized additive model (Zou et al., 2016b), the timely structure adaptive model (Fang et al., 2016), the Gaussian processes model (Yu et al., 2017), the machine learning approach (Liu

* Corresponding author.
E-mail address: jpguocams@gmail.com (J. Guo).

https://doi.org/10.1016/j.atmosenv.2018.09.054
Received 4 August 2018; Received in revised form 21 September 2018; Accepted 25 September 2018
Available online 01 October 2018

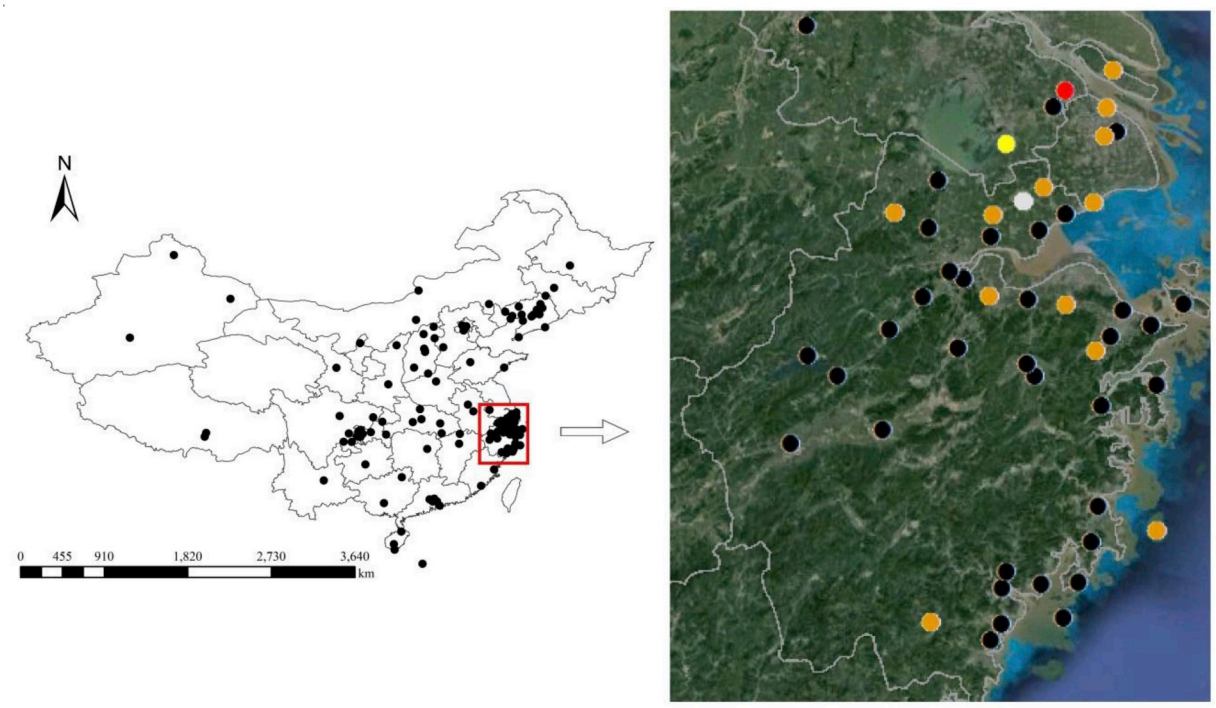

Fig. 1. The distribution of PM_1 observational stations (black dots) in China from the China Atmosphere Watch Network (left panel). The red rectangle represents the Yangtze River Delta region, and the right-hand side panel shows the distribution of PM_1 station over YRD. Black dots represent the stations that have observations for all the four years. Red dots represent the stations that have observations only for 2014, 2015 and 2016. White dots represent the stations that have observations only for 2015 and 2016. Yellow dots represent the stations that have observations only for 2016 and 2017. Orange dots represent the stations that have observations only for 2015, 2016 and 2017. (For interpretation of the references to color in this figure legend, the reader is referred to the Web version of this article.)

et al., 2018b), and the deep learning approach (Li et al., 2017). Notably, the GTWR model that simultaneously reconciles the spatio-temporal variabilities well existing within the variables, is increasingly popular in air quality studies (Qin et al., 2017; He and Huang, 2018a, 2018b).

Compared with $PM_{2.5}$, PM_1, no matter it is from ground-level observation or space-borne estimation, has been less intensively studied. In China, the ground-level PM_1 concentrations are largely measured through the China Atmosphere Watch Network (CAWNET) of the China Meteorological Administration, which consists of about one hundred PM_1 stations across mainland China. More PM_1 stations have been established over past few years. Particularly, 101, 118, 112 and 110 stations were installed in 2014, 2015, 2016 and 2017, respectively (Fig. 1). As a first attempt, Chen et al. (2018) estimated the PM_1 from MODIS AOD in China based on measurements from 77 CAWNET stations from November 2013 to July 2014 using the generalized additive model. Later on, Zang et al. (2018) retrieved the hourly PM_1 concentrations from Himawari-8 aerosol optical depth in China, using the same ground-based PM_1 measurements. Nevertheless, the models they used have limited capability in dealing with small-scale temporal and spatial variability in the PM_1-AOD relationship (He et al., 2018a), even though the variables such as province, month and day of week have been taken to account for the regional and seasonal variations of the PM_1-AOD associations. Therefore, there remains considerable room for improvement of PM_1 estimation.

It is worth noting that the PM_1 stations are unevenly distributed, nearly half of which are concentrated in the Yangtze River Delta (YRD) region, one of the most polluted regions in China (Wang et al., 2012). This gives us an unprecedented opportunity to improve the estimation of PM_1 from MODIS AOD over the YRD region. Therefore, the main purpose of this study is twofold: (1) the GTWR model will be used to estimate PM_1 over the YRD of China, given the fact that this method takes full advantage of spatio-temporal autocorrelation of the PM_1-AOD relationship; (2) the PM_1 data will be produced over the PRD for the period from 2014 to 2017, which is used for preliminary assessment of human exposure to aerosol pollution. The remainder of this paper is organized as follows. Section 2 describes the data and method. Section 3 presents main results of PM_1 estimate from MODIS, and the PM_1 exposure levels are discussed as well, followed by the comparison analyses of PM_1 estimates from 10 km and 3 km MODIS AOD data. The key findings are summarized in section 4.

2. Data and methods

2.1. MODIS aerosol optical depth

The Aqua and Terra MODIS Collection 6 (C6) AOD product at 10 km resolution (at nadir) derived by the Deep Blue (DB) algorithm (DB_{10km}) from January 2014 to December 2017 were obtained from the Goddard Space Flight Center (http://ladsweb.nascom.nasa.gov/data). The MODIS DB algorithm was originally developed for AOD retrievals over bright land (e.g., urban and desert) to fill the gaps left by the Dark Target (DT) algorithm (Hsu et al., 2006). The DB_{10km} AOD product in the MODIS C6 based on the enhanced DB algorithm has been validated and reported better retrieval accuracy than the DT AOD at 10 km resolution (DT_{10km}) product (Sayer et al., 2013; Tao et al., 2015; Bilal et al., 2015). As a supplement to the coarse resolution DT_{10km}, a DT AOD product at 3 km resolution (DT_{3km}) based on the same retrieval algorithm as used in the DT_{10km} is introduced in the MODIS C6 AOD product (Remer et al., 2013; Levy et al., 2013). To estimate the ground PM_1 concentrations at a better spatial resolution, the DT_{3km} and a merged DT and DB AOD product at 3 km resolution (DTB_{3km}) based on the Simplified Merge Scheme (SMS) developed by Bilal et al. (2017a; 2018), from January 2016 to December 2016 were used. Here, only the AOD data at 550 nm with high quality (i.e., Aerosol Confidence Flag = 2, 3, corresponding to good and very good data quality, respectively) have been used in the following paragraphs unless noted otherwise.

2.2. Ground PM_1 measurements

Four years (2014–2017) of ground-level PM_1 data were acquired from the CAWNET. The measurements are conducted using the GRIMM EDM 180 optical laser light aerosol spectrometer, which records the particle size number distribution in 31 size channels between 0.25 μm and 32 μm and converts these results simultaneously to PM_{10}, $PM_{2.5}$, and PM_1 mass concentrations. The GRIMM EDM 180 is operated at a flow rate of 1.2 L/min and 5-min temporal resolution. Details about the measurements and calibration were reported by Guo et al. (2009). To control the data quality, the outliers outside the range of mean plus or minus three standard deviations were screened out. As such, only 37, 45, 48 and 55 PM_1 stations were selected for further analyses in 2014, 2015, 2016 and 2017, respectively.

2.3. Meteorological data

Given the unanimous and significant aerosol-meteorology interaction (Li et al., 2017), the PM retrieval from satellite AOD have to take meteorological variables into account (Liu et al., 2009). Here the meteorological variables, air temperature at 2m above ground (T), relative humidity (RH), planetary boundary layer height (PBLH), wind speed at 10m above ground (WS), and ambient pressure near ground (Pre), were included. All these meteorological variables were obtained from simulations at hourly intervals during the period from 2014 to 2017, using the Weather Research and Forecasting model (WRF version 3.9) that is a mesoscale numerical weather prediction system. The initial and boundary conditions for each simulation experiment were set up based on the National Centre for Environmental Prediction (NCEP) global Final (FNL) reanalysis with a grid spacing of 1° × 1° (http://rda.ucar.edu/datasets/ds083.2/), following the methods proposed by Guo et al. (2016a). Two nested domain schemes with horizontal grid spacing of 30 km and 10 km was applied. The inner domain encompasses the YRD region shown in Fig. 1. The main physical parameterization schemes adopted in the WRF simulation include the single-moment 3-class (WSM3) microphysics, the Rapid Radiative Transfer Model (RRTM) longwave and Dudhia shortwave radiation schemes, the Yonsei University (YSU) PBL scheme, and Noah land surface model. We conducted 48-h simulations for each day of the study period, which started from 0000 UTC of the previous day. For each two-day (48 h) simulation, the former day was considered as a spin-up period, and the latter day was left for further analyses.

2.4. Other data

Global Shuttle Radar Topography Mission (SRTM) Digital Elevation Model (DEM) data at 1 km resolution was downloaded from the CGIAR Consortium for Spatial Information (http://srtm.csi.cgiar.org/). Gridded population data at 1 km resolution was obtained from the Sixth National Population Census of the People's Republic of China for the year 2010 (http://www.stats.gov.cn/ztjc/zdtjgz/zgrkpc/dlcrkpc/dlcrkpczl/).

2.5. Data integration

To integrate the various datasets, MODIS AOD pixels were resampled to the 10 km × 10 km grid and 3km × 3 km grid for 10 km and 3 km AOD observations, respectively, using the nearest neighbor algorithm (Bilal et al., 2017). The PM_1 data from the stations within the corresponding grid during 0200–0300 UTC and 0500-0600 UTC were averaged to match the Terra and Aqua satellite AOD, respectively. The hourly meteorological data during 0200–0300 UTC and 0500-0600 UTC were averaged to match the Terra and Aqua satellite AOD, respectively, which were resampled or interpolated to the 10 km and 3 km grids. Given the range of PBLH in China (Guo et al., 2016c; Zhang et al., 2018), the raw dataset with the PM_1 concentration < 1 μg/m^3 and the PBLH < 200m were excluded for further analyses. Finally, 16,756 matched datasets, co-located in both space and time from 1 January 2014 to 31 December 2017, were included in the model development for 10 km PM_1 estimation, and 4054 matched datasets from 1 January to 31 December 2016 were used for 3 km PM_1 estimation. Descriptive statistics of all the variables used in the 10 km PM_1 estimation are summarized in Table S1. Overall, the average ground-level PM_1 concentration is as high as 35.08 μg/m^3 with a large standard deviation of 25.16 μg/m^3, exhibiting a large variability ranging from 1.28 μg/m^3 to 302.14 μg/m^3. Correspondingly, the DB_{10km} AOD data have a mean value of 0.36, but with a high standard deviation of 0.35.

2.6. GTWR model development and evaluation

To construct the GTWR model, a few of meteorological variables, DEM and population data were used as inputs to the model. Taking the aforementioned variables into account, the relationship of ground PM_1 concentrations and satellite AOD in the GTWR model can be simply expressed as:

$$\begin{aligned} PM_{1(i)} = {} & \beta_0(u_i, v_i, t_i) + \beta_1(u_i, v_i, t_i)AOD_{(i)} + \beta_2(u_i, v_i, t_i)RH_{(i)} + \beta_3(u_i, v_i, t_i)T_{(i)} \\ & + \beta_4(u_i, v_i, t_i)PBLH_{(i)} + \beta_5(u_i, v_i, t_i)WS_{(i)} + \beta_6(u_i, v_i, t_i)Pre_{(i)} \\ & + \beta_7(u_i, v_i, t_i)DEM_{(i)} + \beta_8(u_i, v_i, t_i)Pop_{(i)} + \varepsilon_i (i = 1,2,...,n) \end{aligned} \quad (1)$$

where $PM_{1(i)}$ represents the ground-measured PM_1 concentration for sample i at time t_i at location (u_i, v_i); $\beta_0(u_i, v_i, t_i)$ stands for the intercept, $\beta_1(u_i, v_i, t_i)$, $\beta_2(u_i, v_i, t_i)$, $\beta_3(u_i, v_i, t_i)$, $\beta_4(u_i, v_i, t_i)$, $\beta_5(u_i, v_i, t_i)$, $\beta_6(u_i, v_i, t_i)$ and $\beta_7(u_i, v_i, t_i)$ are the slopes of AOD, RH, T, PBLH, WS, P, and DEM, respectively, and is the random error (ε ~ N(0.0155, 7.9027^2)).

The spatio-temporal weight matrix $\mathbf{W}(u_0, v_0, t_0)$ (Huang et al., 2010) based on Gaussian distance decay-based functions and Euclidean distance, was used to estimate the intercept and slope. The spatio-temporal distance between two samples was calculated following Huang et al. (2010).

We applied a 10-fold cross validation (CV) to evaluate the model performance. The original samples were randomly partitioned into 10 equal-size subsets. Of the 10 subsets, a single subset was retained as the validation data for testing the model, and the remaining 9 subsets were used as training data. This step was then repeated 10 times until every fold was tested. Furthermore, the coefficient of determination (R^2) and root mean square error (RMSE) were used to evaluate the model accuracy by comparing the satellite-estimated PM_1 concentration with ground PM_1 measurements. The R^2 is an indicator of the explained variation of the satellite-estimated PM_1 to the observed PM_1 concentrations. The RMSE describes how the estimation uncertainty is sensitive to systematic and random errors. The R^2 and RMSE are calculated following Equations (2) and (3), respectively.

$$R^2 = 1 - \frac{\sum_{i=1}^{n} (PM_1^{obs}{}_{(i)} - PM_1^{sat}{}_{(i)})^2}{\sum_{i=1}^{n} (PM_1^{obs}{}_{(i)} - \overline{PM_1^{obs}})^2} \quad (2)$$

where n is the number of ground observation, PM_1^{obs} and $\overline{PM_1^{obs}}$ represents the original and averaged concentration of ground observed PM_1, respectively, and PM_1^{sat} denotes for the concentration of satellite-estimated ground-level PM_1.

$$RMSE = \sqrt{\frac{1}{n}\sum_{i=1}^{n} (PM_1^{obs}{}_{(i)} - PM_1^{sat}{}_{(i)})^2} \quad (3)$$

3. Results and discussion

3.1. General performances of GTWR model

Fig. 2 shows the scatterplots between ground-measured and satellite-estimated PM_1 concentrations. The R^2 value is found to reach as

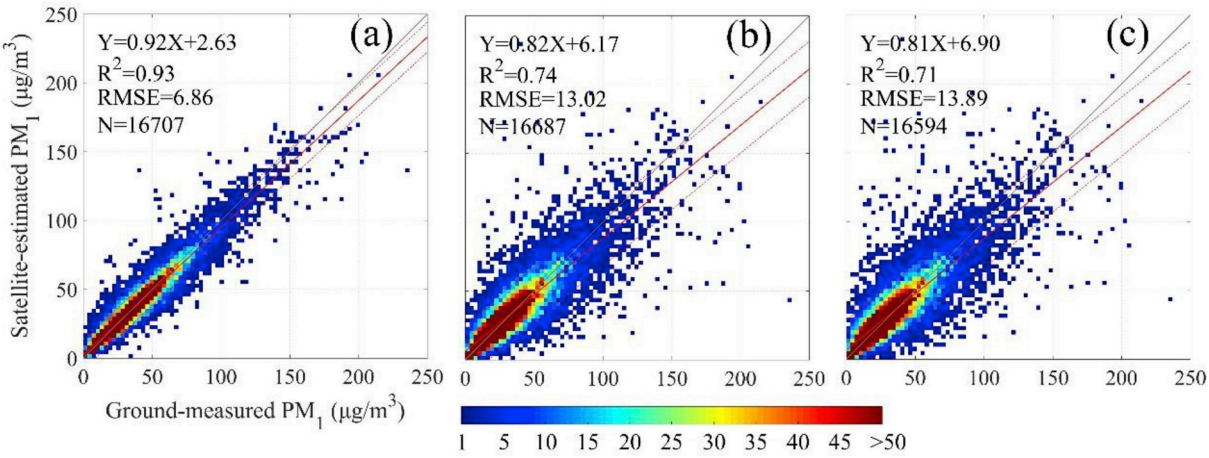

Fig. 2. Scatterplots between ground-measured and satellite-estimated PM_1 concentrations using the GTWR model, based on (a) fitting dataset, (b) validation dataset, and (c) validation dataset with AOD errors. The black solid line is the 1:1 line as a reference, the red solid line is the trend line and the red dash lines are the 95% confidence intervals. The color bar indicates the number of data points. Note that Terra and Aqua satellite AOD, PM_1 and other variables spatiotemporally matched with each other were included here. (For interpretation of the references to color in this figure legend, the reader is referred to the Web version of this article.)

Table 1
Model performances for cross validation of PM_1 estimation with selected variables.

Variable	Slope	Intercept	R^2	RMSE (μg/m^3)
AOD	0.60	13.76	0.62	15.43
AOD + PBLH	0.65	12.09	0.66	14.71
AOD + PBLH + T	0.69	10.73	0.68	14.23
AOD + PBLH + T + WS	0.72	9.51	0.70	13.82
AOD + PBLH + T + WS + RH	0.76	8.39	0.71	13.52
AOD + PBLH + T + WS + RH + Pre	0.79	7.35	0.72	13.42
AOD + PBLH + T + WS + RH + Pre + DEM	0.81	6.48	0.73	13.28
AOD + PBLH + T + WS + RH + Pre + DEM + Pop	0.82	6.17	0.74	13.02

Note: AOD is aerosol optical depth; PBLH is planetary boundary layer height; T is air temperature at 2m above ground; WS is wind speed at 10m above ground; RH is relative humidity; Pre is ambient pressure near ground; DEM is digital elevation model; Pop is population. Terra and Aqua satellite AOD, PM_1 and other variables spatiotemporally matched with each other were included in this dataset.

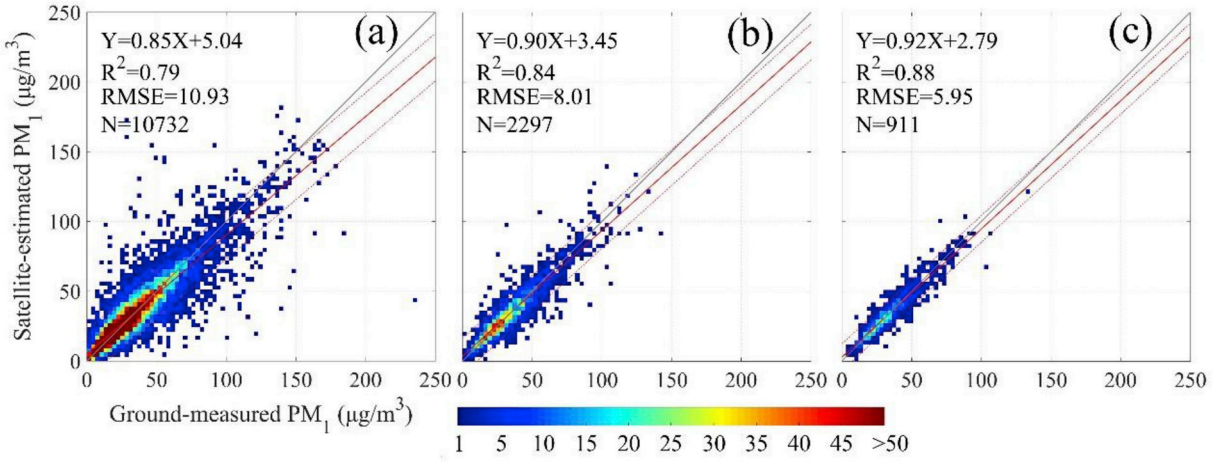

Fig. 3. Scatterplots between ground-measured and satellite-estimated PM_1 concentrations using GTWR model, based on (a) daily validation dataset, (b) monthly validation dataset, and (c) seasonal validation dataset. The black solid line is the 1:1 line as a reference, the red solid line is the trend line and the red dash lines are the 95% confidence intervals. The color bar indicates the number of data points. Note that daily, monthly, and seasonal datasets were averaged from the Aqua and Terra MODIS estimated PM_1. (For interpretation of the references to color in this figure legend, the reader is referred to the Web version of this article.)

high as 0.93 and the RMSE 6.86 μg/m^3 for model fitting (Fig. 2a), while they are 0.74 and 13.02 μg/m^3 respectively for model validation (Fig. 2b), suggesting an over-fitting. Basically, our R^2 value is similar to the validation R^2 of 0.725 for $PM_{2.5}$ estimation over the YRD region using a nested linear mixed effects model (Ma et al., 2016a,b). The slopes of 0.92 and 0.82 for model fitting and validation indicate a little underestimated. Table 1 shows the step-by-step performances of PM_1 estimation for model validation with the addition of each consecutive variable. As expected, the AOD-only model produces a promising result (R^2 = 0.62, RMSE = 15.4 μg/m^3), since the satellite AOD is the dominant predictor for PM estimations. The error in satellite AOD may cause over-/under-estimation of PM concentrations. Tao et al. (2015) found

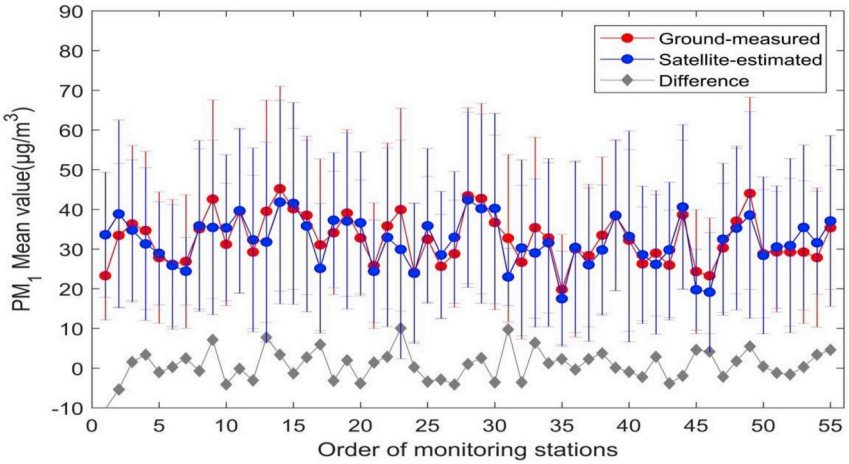

Fig. 4. Annual average PM_1 concentrations from satellite-estimated (0200-0300 UTC and 0500-0600 UTC) and ground-measured (24 h) during the period 2014 to 2017 for 55 ground stations.

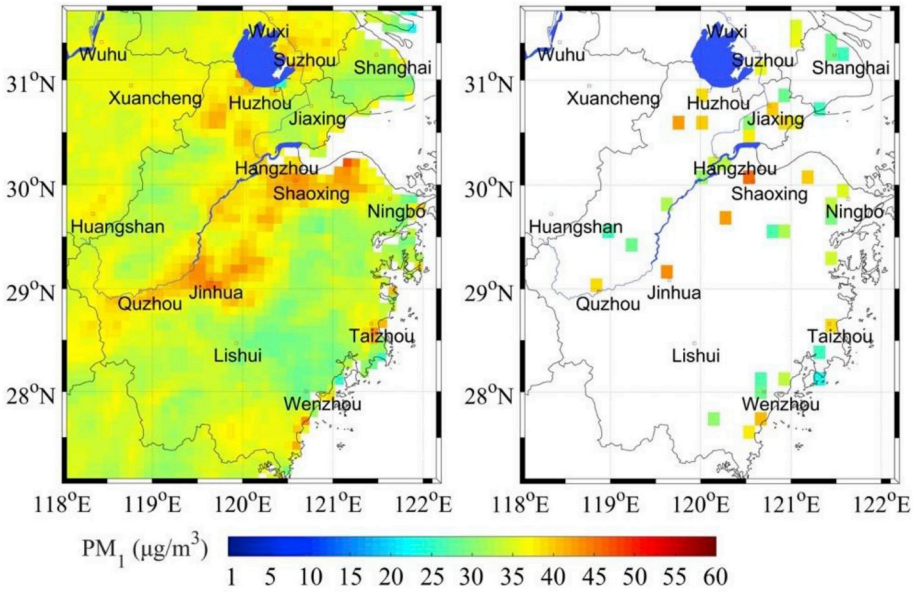

Fig. 5. Spatial distribution of average PM_1 concentrations during the period 2014 to 2017 over the YRD region from satellite-estimated (left) and ground-measured (right). Note that the area of Taihu Lake between Wuxi, Shuzhou and Huzhou are masked as blue (null value) due to near unavailability of MODIS AOD retrievals over turbid waters. (For interpretation of the references to color in this figure legend, the reader is referred to the Web version of this article.)

Table 2
Model performances for cross validation of PM_1 estimations of different seasons.

Season	Slope	Intercept	R^2	RMSE (μg/m^3)
Spring	0.77	7.86	0.68	12.56
Summer	0.77	5.53	0.63	11.39
Autumn	0.79	6.20	0.70	11.85
Winter	0.82	9.02	0.75	16.07

Table 3
Model performances for cross validation of PM_1 estimations of different years.

Year	Slope	Intercept	R^2	RMSE (μg/m^3)
2014	0.81	8.26	0.71	16.36
2015	0.83	6.37	0.76	13.27
2016	0.80	6.28	0.73	11.70
2017	0.81	5.66	0.72	11.57

that the MODIS C6 DB_{10km} AOD retrievals at Hangzhou had an RMSE of 0.251 as compared to the ground-based sunphotometer observations. For the sensitivity analysis, we introduced normally distributed AOD errors with a mean of zero and a standard deviation of 0.251 to the model. As the comparison results shown in Fig. 2(b)-2(c), the uncertainty of our model was very small in terms of expected errors from the MODIS AOD. The other variables made similar contributions and gradually improved the model performance (Table 1), i.e. the R^2 and the slope increased, where the RMSE and the intercept decreased.

Moreover, Aqua and Terra MODIS estimated PM_1 were averaged to get daily PM_1 concentrations, and further averaged to get monthly and seasonal PM_1 concentrations. The model validation result shows an improved predictive ability for daily estimations (R^2 = 0.79 and RMSE = 10.93 μg/m^3, Fig. 3a), monthly estimations (R^2 = 0.84 and RMSE = 8.01 μg/m^3, Fig. 3b) and seasonal estimations (R^2 = 0.88 and RMSE = 5.95 μg/m^3, Fig. 3c). These are much better than the results across China by Chen et al. (2018a), which reported the R^2 values of 0.59, 0.71 and 0.77 for daily, monthly and seasonal mean PM_1, respectively.

It should be noted that the daily estimations are only based on the data averaged over the estimations during 0200–0300 UTC and 0500-0600 UTC. Fig. 4 present a comparison of annual average satellite-estimated PM_1 concentrations during 2014–2017 and the corresponding ground observations averaged over 24-h data. Almost all of the stations possess low mean discrepancies of less than 10 μg/m^3.

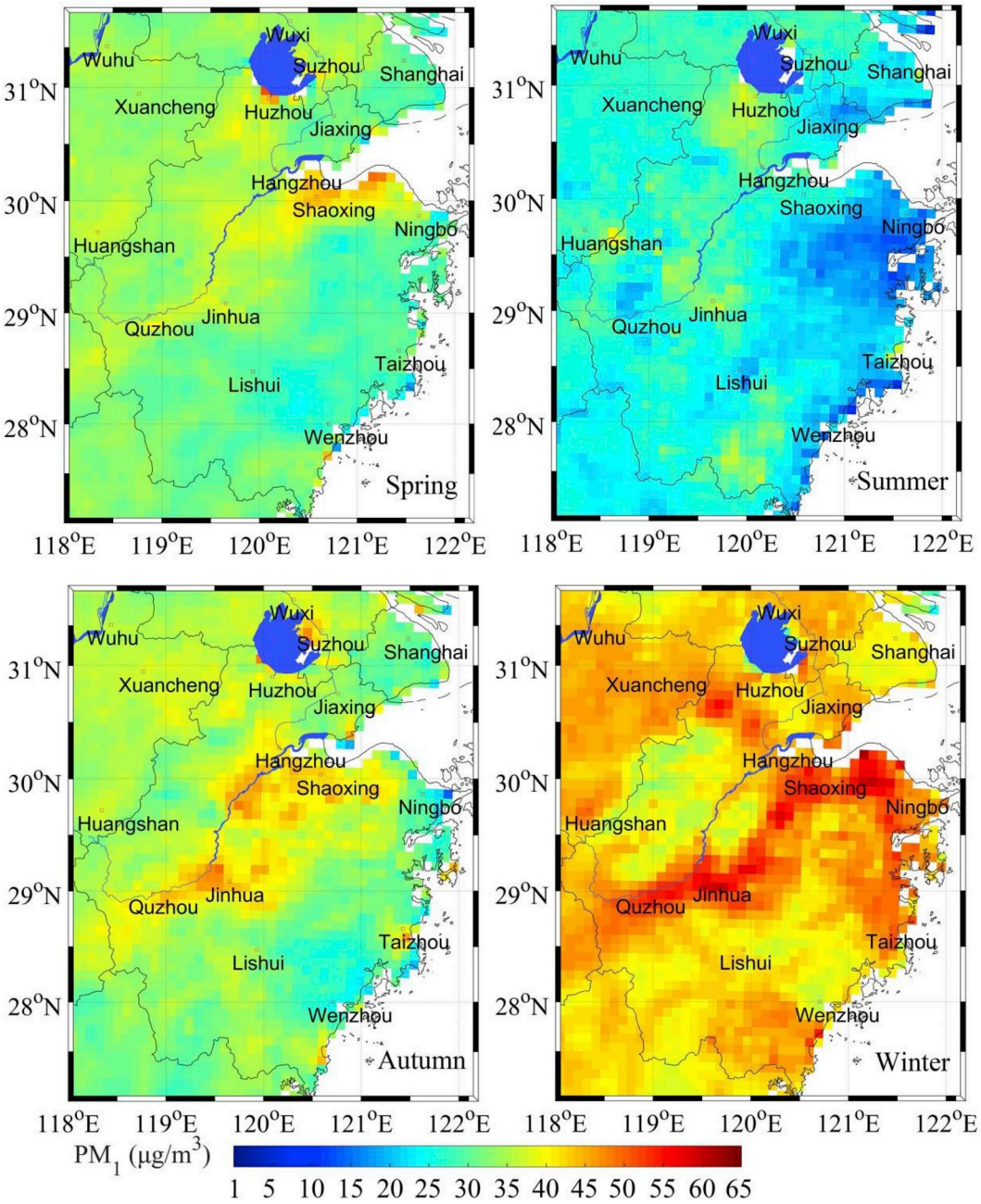

Fig. 6. Spatial distribution of seasonal average satellite-estimated PM_1 concentrations during the period 2014 to 2017 over the YRD region. Note that the area of Taihu Lake between Wuxi, Shuzhou and Huzhou are masked as blue (null value) due to nearly unavailability of MODIS AOD retrievals over turbid waters. (For interpretation of the references to color in this figure legend, the reader is referred to the Web version of this article.)

As shown in Fig. 5, the spatial patterns of satellite-estimated and ground-observed PM_1 mean concentrations during the period 2014 to 2017 are highly consistent with each other. It demonstrates that contiguous high PM_1 areas are mainly distributed in the cities of north Zhejiang province and Jinhua-Quzhou basin, whereas mountains have low PM_1 concentration. Obviously, satellite approach can obtain the spatial variations of surface PM_1 concentrations where the ambient monitoring stations are sparse and unevenly distributed. It is worth noting that the megacity of Shanghai possesses relatively low PM_1, which is different from the high $PM_{2.5}$ in previous studies (e.g. Ma et al., 2016a,b). This could be attributed to different proportions of PM_1 and $PM_{2.5}$ emitted from various sources (Wang et al., 2010; Chen et al., 2018a). The four-years averaged PM_1 concentrations over the YRD region ranged from 19.99 μg/m^3 to 47.66 μg/m^3, with a spatial mean value of 34.76 ± 2.47 μg/m^3.

3.2. Seasonal and inter-annual variations of PM_1

In addition, we assessed our PM_1 estimations for different seasons and years, which is summarized in Tables 2 and 3, and presented the seasonal and inter-annual variations in Figs. 6 and 7, respectively. Our analyses yield seasonal validation R^2 values of 0.68, 0.63, 0.70 and 0.75 for spring, summer, autumn and winter, respectively, slightly higher than those for satellite-based $PM_{2.5}$ estimations over the YRD region by Zheng et al. (2016). The spatial distributions of seasonal mean PM_1 concentrations (Fig. 6) displays the highest values in winter (mean = 43.55 μg/m^3, maximum = 61.35 μg/m^3) and the lowest in summer (mean = 24.38 μg/m^3, maximum = 39.96 μg/m^3). Spring and

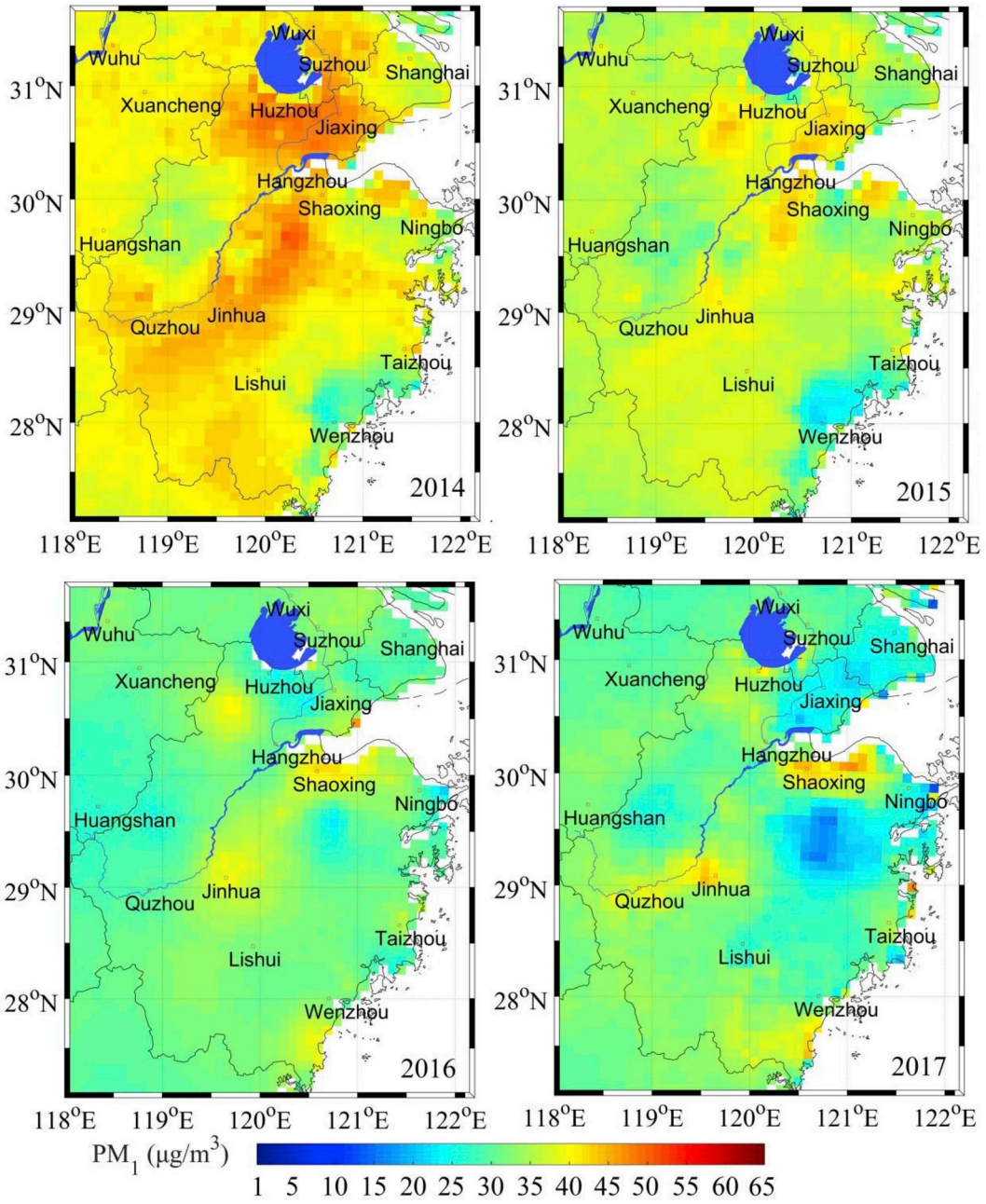

Fig. 7. Spatial distribution of annual mean satellite-estimated PM_1 concentrations during the period 2014 to 2017 over the YRD region. Note that the area of Taihu Lake between Wuxi, Shuzhou and Huzhou are masked as blue (null value) due to nearly unavailability of MODIS AOD retrievals over turbid waters. (For interpretation of the references to color in this figure legend, the reader is referred to the Web version of this article.)

autumn have approximate seasonal mean values of 32.84 μg/m^3 and 33.96 μg/m^3, respectively. This seasonal variation is generally consistent with the conclusion by Chen et al. (2018b) who analyzed ground-measured data from 96 PM_1 stations in China for the period from November 2013 to December 2014. The difference in the spatial distribution of seasonal average PM_1 could relate to the variation of local anthropogenic emissions, such as diesel emissions, gasoline emissions and coal combustion (e.g., Tao et al., 2012) and meteorological conditions (PBLH, wind, pressure, temperature and precipitation, etc.), as well as regional transportation of biomass burning aerosols (e.g., Tang et al., 2016).

As presented in Table 3, the evaluation metrics (namely, R^2, slope, intercept, and RMSE) of the PM_1 estimations for different years are very close to each other for each year, indicting a stable model performance. Fig. 7 presents the spatial distribution of the annual average PM_1, which exhibits an overall year-by-year decline from 2014 to 2016, with spatial mean values of 39.94 ± 2.97 μg/m^3, 35.66 ± 2.58 μg/m^3, and 30.84 ± 2.18 μg/m^3 for 2014, 2015, and 2016, respectively. The level of PM_1 in 2017 was similar to that in 2016.

3.3. Population exposure to PM_1

Given the adverse PM_1 impact on human health, it is imperative to evaluate long-term population exposure levels over different prefecture-level cities in the YRD regions for the period from 2014 to 2017. We calculated the four-years population-weighted mean PM_1 (MPPM1) concentrations using the following formula.

$$MPPM1^j = \frac{\sum_i^N Population^{j,i} \times PM_1^{j,i}}{\sum_i^N Population^{j,i}} \quad (4)$$

Table 4
Population-weighted PM_1 concentration during the period 2014 to 2017 for 16 prefecture-level cities in the YRD region.

City/region	Population-weight Mean (μg/m^3)	The proportion of people exposed to high-level PM_1 concentrations (> 35 μg/m^3)
Ningbo	53.23	46.89
Wuxi	48.77	94.04
Shaoxing	47.86	47.83
Jinhua	40.92	80.15
Huangshan	39.67	82.87
Huzhou	39.04	76.17
Shanghai	32.50	0
Quzhou	37.98	93.47
Hangzhou	37.47	51.32
Xuancheng	37.28	96.94
Wuhu	36.56	100
Suzhou	36.16	78.59
Taizhou	35.6	34.09
Lishui	35.51	4.85
Jiaxing	34.13	18.33
Wenzhou	30.93	44.64
YRD	30.93	44.64

where $MPPM1^j$ is the population-weighted PM_1 for the city j, $PM_1^{j,i}$ and $Population^{j,i}$ are the PM_1 concentration and population data of the pixel i in the city j respectively.

The population-weighted mean PM_1 concentration over the YRD regions is 37.22 μg/m^3 (Table 4). The highest levels of PM_1 exposure occurred at Ningbo with the value of 53.23 μg/m^3, while the lowest exposure occurred at, Wenzhou with the value of 30.93 μg/m^3. Currently, there is no air quality standard for PM_1 concentration. Therefore, we used the World Health Organization Air Quality Interim Target-1 of 35 μg/m^3 for $PM_{2.5}$ as the standard of high-level PM_1 (World Health Organization, 2006). Near half of total population in the YRD region inhabits in places with high-level PM_1 levels. People from Wuxi, Jinhua, Huangshan, Quzhou, Xuancheng and Wuhu suffer from the most serious PM_1 pollution, with more than 80% of people affected by high-level PM_1 concentrations. These findings could help to evaluate the long-term effects of PM_1 air pollution and disease burden attributed to PM_1 exposures over the YRD region in China.

3.4. Comparisons using 10 km and 3 km AOD datasets

The satellite-based ground-level PM_1 estimation at a higher spatial resolution facilitates our explicit and full understanding of population exposures to aerosol pollution. First of all, it is imperative to see the performance discrepancy of PM_1 retrievals from MODIS at two different grid sizes. The MODIS C6 DT AOD product at 3 km (DT_{3km}) has been used to estimate $PM_{2.5}$ concentrations (Xie et al., 2015; Bilal et al., 2017b). However, the DT_{3km} product exhibits larger errors than the DT_{10km} product due to the errors in the estimated surface reflectance (Remer et al., 2013; Nichol and Bilal, 2016). Bilal et al. (2018) developed a new DT and DB merged AOD product at 3 km resolution (DTB_{3km}) using the DT_{3km} AOD and DB_{3km} AOD resampled from the DB_{10km} using the nearest neighbor algorithm, supplement with high-resolution information over dense vegetation regions where DT_{3km} is susceptible to error. As compared in Fig. 8, the PM_1 estimations using the DTB_{3km} product yields the best result (namely, the highest value of R^2, the most number of matched dataset, and the lowest value of RMSE), while the DB_{10km} is the second, and the DT_{3km} is the worst. This could be attributed to more matched samples and smaller retrieval errors in the DTB_{3km} AOD. Comparing Fig. 9a and Fig. 9b demonstrates that the 3 km PM_1 map from the DTB_{3km} provides more details than those from the DT_{10km}. Notably, Fig. 9b shows that a gradual change in PM_1 concentration occurs from southern to central Zhejiang province (e.g., Jinhua-Quzhou basin), while it is a sudden change (Fig. 9a) due to coarse resolution of AOD. These results suggest that the DTB_{3km} significantly improves the PM_1 estimation with more AOD retrievals in revealing the local-level spatial variability of PM_1 concentration.

4. Summary and concluding remarks

In this paper, the geographically and temporally weighted regression (GTWR) model that can better characterize the spatial and temporal variability between aerosol optical depth (AOD) and particulate matter (PM), were used to estimate ground-level PM_1 concentrations over the YRD region, based on hourly ground-based PM_1 measurements over the PRD of China, along with MODIS C6 Deep Blue AOD at 10 km resolution (DB_{10km}), Weather Research and Forecasting model (WRF) simulated meteorological data, digital elevation model (DEM) and population data.

In general, the satellite-based PM_1 estimated from the GTWR model showed a good agreement with ground-level PM_1 measurements with R^2 value of 0.74 and RMSE value of 13.02 μg/m^3 for model validation. It also exhibited a reasonable and representative pattern in terms of the regional variability of PM_1 over the YRD region, similar to that from ground measurements. The highest PM_1 level was found in winter with the largest R^2. The PM_1 level continuously declined from 2014 to 2016, but remained stable during the period from 2016 to 2017. The

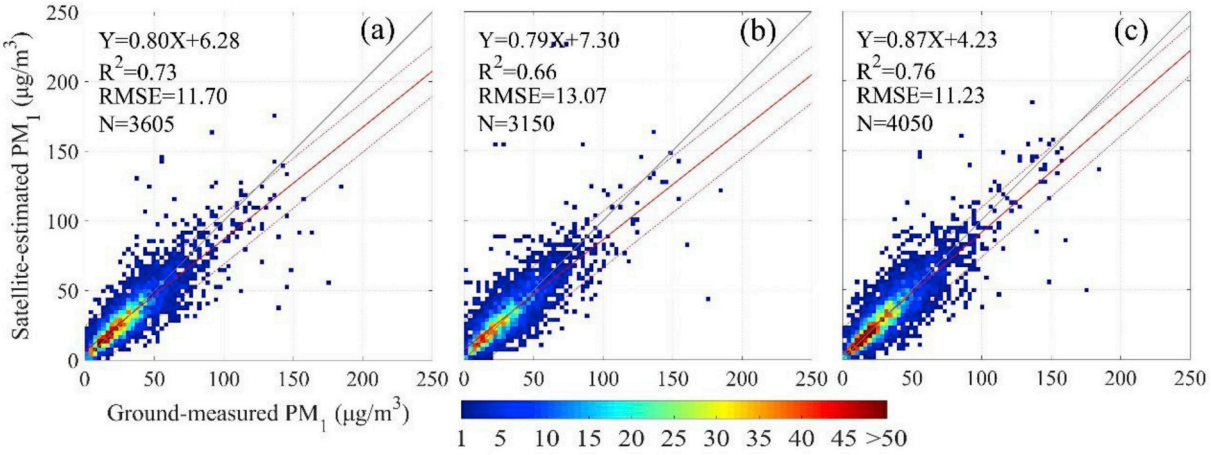

Fig. 8. Scatterplots between ground-measured and satellite-estimated PM_1 concentrations using GTWR model, based on validation dataset in 2016 for (a) MODIS DB_{10km} AOD, (b) MODIS DT_{3km} AOD, and (c) MODIS DTB_{3km} AOD. The black solid line is the 1:1 line as a reference, the red solid line is the trend line and the red dash lines are the 95% confidence intervals. The color bar indicates the number of data points. (For interpretation of the references to color in this figure legend, the reader is referred to the Web version of this article.)

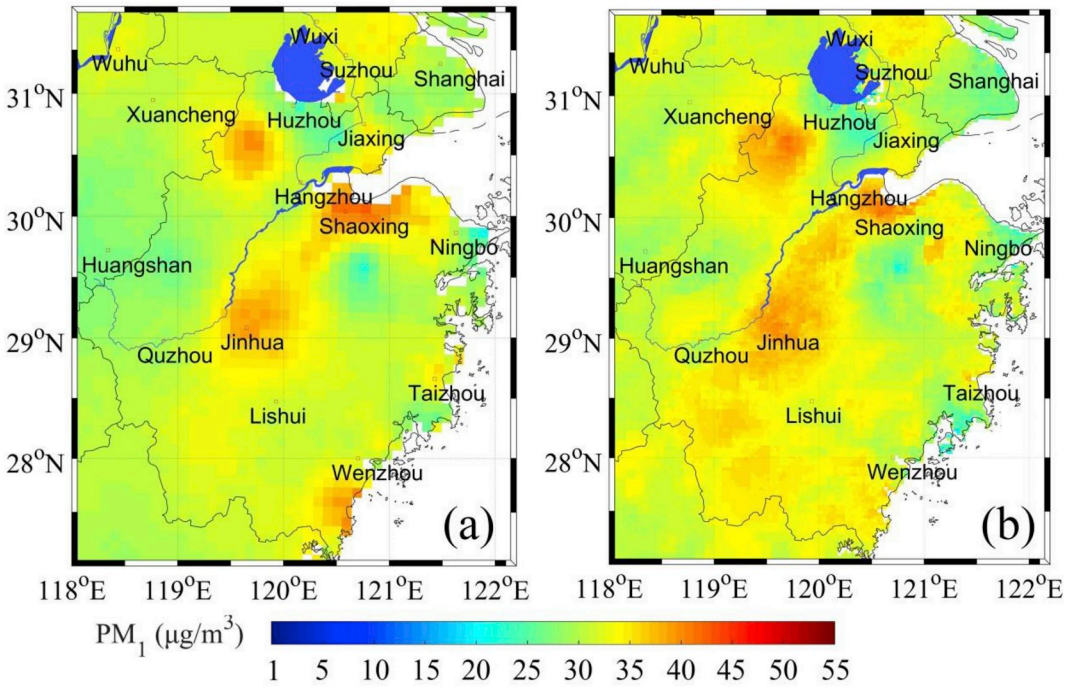

Fig. 9. Spatial distributions of annual PM_1 in 2016 estimated using (a) MODIS DB_{10km} AOD, and (b) MODIS DTB_{3km} AOD. Note that the area of Taihu Lake between Wuxi, Shuzhou and Huzhou are masked as blue (null value) due to nearly unavailability of MODIS AOD retrievals over turbid waters. (For interpretation of the references to color in this figure legend, the reader is referred to the Web version of this article.)

population-weighted mean of PM_1 concentrations over the YRD region was 37.93 μg/m^3 and near half the people lived in locations with high-level PM_1 concentration (> 35 μg/m^3). A new merged MODIS Dark Target and Deep Blue AOD product at 3 km resolution (DTB_{3km}) based on the simplified merged scheme (Bilal et al., 2017, 2018), yielded a better PM_1 estimation result than the DB_{10km} and the MODIS C6 Dark Target AOD at 3 km resolution (DT_{3km}). Overall, the present work improves much over previous similar work regarding the accuracy of satellite-estimated PM_1 concentrations.

In the long end, the results obtained here could help to evaluate the long-term effects of PM_1 air pollution on disease burden over the YRD region in China. In future studies, the new merged DTB_{3km} could be used to elucidate the spatial and temporal variability of PM_1 in more details.

Acknowledgments

This study was supported by the Fundamental Research Funds for the Central Universities under grant 2015XKMS049, the National Natural Science Foundation of China under grants 41730109 and 91544217, and the National Key R&D Program of China under grant 2017YFC1501401. We would like to acknowledge NASA for making the MODIS AOD data publicly accessible. Also, we appreciate the National Centre for Environmental Prediction (NCEP) global Final (FNL) reanalysis provided by UCAR (http://rda.ucar.edu/datasets/ds083.2/). Last but not least, special thanks go to the anonymous referees for their constructive and kind comments that help much improve the quality of this work.

Appendix A. Supplementary data

Supplementary data to this article can be found online at https://doi.org/10.1016/j.atmosenv.2018.09.054.

References

Agudelo-Castañeda, D.M., Teixeira, E.C., Schneider, I.L., et al., 2017. Exposure to polycyclic aromatic hydrocarbons in atmospheric $PM_{1.0}$ of urban environments: carcinogenic and mutagenic respiratory health risk by age groups. Environ. Pollut. 224, 158–170.

Bai, Y., Wu, L., Qin, K., et al., 2016. A geographically and temporally weighted regression model for ground-level PM2.5 estimation from satellite-derived 500m resolution AOD. Rem. Sens. 8 (3), 262.

Beckerman, B.S., Jerrett, M., Serre, M., et al., 2013. A hybrid approach to estimating national scale spatiotemporal variability of PM2.5 in the contiguous United States. Environ. Sci. Technol. 47 (13), 7233–7241.

Bilal, M., Nichol, J.E., 2015. Evaluation of MODIS aerosol retrieval algorithms over the Beijing-Tianjin-Hebei region during low to very high pollution events. J. Geophys. Res.: Atmosphere 120 (15), 7941–7957.

Bilal, M., Nichol, J.E., Wang, L., 2017a. New customized methods for improvement of the MODIS C6 Dark Target and Deep Blue merged aerosol product. Remote Sens. Environ. 197, 115–124.

Bilal, M., Nichol, J.E., Spak, S.N., 2017b. A new approach for estimation of fine particulate concentrations using satellite aerosol optical depth and binning of meteorological variables. Aerosol Air Qual Res.. 17 (2), 356–367.

Bilal, M., Qiu, Z., Campbell, J.R., et al., 2018. A new MODIS C6 Dark Target and deep blue merged aerosol product on a 3 km spatial grid. Rem. Sens. 10 (3), 463.

Che, H., Xia, X., Zhu, J., et al., 2014. Column aerosol optical properties and aerosol radiative forcing during a serious haze-fog month over North China Plain in 2013 based on ground-based sunphotometer measurements. Atmos. Chem. Phys. 14 (4), 2125–2138.

Chen, Z., Liu, C., Liu, W., et al., 2017a. A synchronous observation of enhanced aerosol and NO_2 over Beijing, China, in winter 2015. Sci. Total Environ. 575, 429–436.

Chen, G., Li, S., Zhang, Y., et al., 2017b. Effects of ambient PM_1 air pollution on daily emergency hospital visits in China: an epidemiological study. Lancet Planet Earth 1 (6), 221–229.

Chen, G., Knibbs, L.D., Zhang, W., et al., 2018a. Estimating spatiotemporal distribution of PM_1 concentrations in China with satellite remote sensing, meteorology, and land use information. Environ. Pollut. 233, 1086–1094.

Chen, G., Morawska, L., Zhang, W., et al., 2018b. Spatiotemporal variation of PM_1 pollution in China. Atmos. Environ. 178, 198–205.

Cohen, A.J., Brauer, M., Burnett, R., et al., 2017. Estimates and 25-year trends of the global burden of disease attributable to ambient air pollution: an analysis of data from the Global Burden of Diseases Study 2015. Lancet 389 (10082), 1907–1918.

Fang, X., Zou, B., Liu, X., Sternberg, T., Zhai, L., 2016. Satellite-based ground $PM_{2.5}$ estimation using timely structure adaptive modeling. Remote Sens. Environ. 186, 152–163.

Guo, J.P., Zhang, X.Y., Che, H.Z., et al., 2009. Correlation between PM concentrations and aerosol optical depth in eastern China. Atmos. Environ. 43 (37), 5876–5886.

Guo, J.P., He, J., Liu, H.L., Miao, Y.C., Liu, H., Zhai, P.M., 2016a. Impact of various emission control schemes on air quality using WRF-Chem during APEC China 2014. Atmos. Environ. 140, 311–319.

Guo, J., Liu, H., Wang, F., Huang, J., Xia, F., Lou, M., Wu, Y., Jiang, J., Xie, T., Zhaxi, Y.,

Yung, Y., 2016b. Three-dimensional structure of aerosol in China: a perspective from multi-satellite observations. Atmos. Res. 178–179, 580–589. https://doi.org/10.1016/j.atmosres.2016.05.010.
Guo, J., Miao, Y., Zhang, Y., Liu, H., Li, Z., Zhang, W., He, J., Lou, M., Yan, Y., Bian, L., Zhai, P., 2016. The climatology of planetary boundary layer height in China derived from radiosonde and reanalysis data. Atmos. Chem. Phys. 16, 13309–13319. https://doi.org/10.5194/acp-16-13309-2016.
Guo, J., Xia, F., Zhang, Y., et al., 2017. Impact of diurnal variability and meteorological factors on the $PM_{2.5}$-AOD relationship: implications for $PM_{2.5}$ remote sensing. Environ. Pollut. 221, 94–104.
Gupta, P., Christopher, S.A., Wang, J., et al., 2006. Satellite remote sensing of particulate matter and air quality assessment over global cities. Atmos. Environ. 40 (30), 5880–5892.
Gupta, P., Christopher, S.A., Box, M.A., et al., 2007. Multiyear satellite remote sensing of particulate matter air quality over Sydney, Australia. Int. J. Rem. Sens. 28 (20), 4483–4498.
Gu, Y., Wong, T.W., Law, S.C.K., et al., 2018. Impacts of sectoral emissions in China and the implications: air quality, public health, crop production, and economic costs. Environ. Res. Lett. 13 (8), 084008.
Gu, Y., Yim, S.H.L., 2016. The air quality and health impacts of domestic trans-boundary pollution in various regions of China. Environ. Int. 97, 117–124.
Geng, G., Zhang, Q., Martin, R.V., et al., 2015. Estimating long-term PM2.5 concentrations in China using satellite-based aerosol optical depth and a chemical transport model. Remote Sens. Environ. 166, 262–270.
Hu, X., Waller, L.A., Lyapustin, A., et al., 2014. Estimating ground-level PM2. 5 concentrations in the Southeastern United States using MAIAC AOD retrievals and a two-stage model. Remote Sens. Environ. 140, 220–232.
Huang, B., Wu, B., Barry, M., 2010. Geographically and temporally weighted regression for modeling spatio-temporal variation in house prices. Int. J. Geogr. Inf. Sci. 24 (3), 383–401.
Hsu, N.C., Tsay, S.C., King, M.D., et al., 2006. Deep blue retrievals of Asian aerosol properties during ACE-Asia. IEEE Trans. Geosci. Rem. Sens. 44 (11), 3180–3195.
He, Q., Huang, B., 2018a. Satellite-based high-resolution PM2.5 estimation over the Beijing-Tianjin-Hebei region of China using an improved geographically and temporally weighted regression model. Environ. Pollut. 236, 1027–1037.
He, Q., Huang, B., 2018b. Satellite-based mapping of daily high-resolution ground PM2.5 in China via space-time regression modeling. Remote Sens. Environ. 206, 72–83.
Ho, H.C., Wong, M.S., Yang, L., et al., 2017. Influences of socioeconomic vulnerability and intra-urban air pollution exposure on short-term mortality during extreme dust events. Environ. Pollut. 235, 155.
Just, A.C., Wright, R.O., Schwartz, J., et al., 2015. Using high-resolution satellite aerosol optical depth to estimate daily PM2.5 geographical distribution in Mexico City. Environ. Sci. Technol. 49 (14), 8576–8584.
Kloog, I., Nordio, F., Coull, B.A., et al., 2012. Incorporating local land use regression and satellite aerosol optical depth in a hybrid model of spatiotemporal PM2.5 exposures in the Mid-Atlantic states. Environ. Sci. Technol. 46 (21), 11913–11921.
Lee, H.J., Liu, Y., Coull, B.A., et al., 2011. A novel calibration approach of MODIS AOD data to predict PM2.5 concentrations. Atmos. Chem. Phys. 11 (15), 7991.
Li, T., Shen, H., Yuan, Q., et al., 2017. Estimating ground-level PM2.5 by fusing satellite and station observations: a geo-intelligent deep learning approach. Geophys. Res. Lett. 44 (23).
Li, Z., Guo, J., Ding, A., et al., 2017. Aerosol and boundary-layer interactions and impact on air quality. Nat. Sci. Rev. 4 (6), 810–833. https://doi.org/10.1093/nsr/nwx117.
Liu, Y., Sarnat, J.A., Kilaru, V., et al., 2005. Estimating ground-level PM2.5 in the eastern United States using satellite remote sensing. Environ. Sci. Technol. 39 (9), 3269–3278.
Liu, Y., Franklin, M., Kahn, R., et al., 2007. Using aerosol optical thickness to predict ground-level PM2.5 concentrations in the St. Louis area: a comparison between MISR and MODIS. Remote Sens. Environ. 107 (1–2), 33–44.
Liu, Y., Paciorek, C.J., Koutrakis, P., 2009. Estimating regional spatial and temporal variability of PM2.5 concentrations using satellite data, meteorology, and land use information. Environ. Health Perspect. 117 (6), 886.
Liu, Y., Cao, G., Zhao, N., et al., 2018. Improve ground-level $PM_{2.5}$ concentration mapping using a random forests-based geostatistical approach. Environ. Pollut. 235, 272–282.
Liu, Z., Yim, S.H.L., Wang, C., et al., 2018. The impact of the aerosol direct radiative forcing on deep convection and air quality in the Pearl River Delta region. Geophys. Res. Lett. 45 (9), 4410–4418.
Lin, C., Li, Y., Lau, A.K.H., et al., 2016. Estimation of long-term population exposure to PM2.5 for dense urban areas using 1-km MODIS data. Remote Sens. Environ. 179, 13–22.
Levy, R.C., Mattoo, S., Munchak, L.A., et al., 2013. The Collection 6 MODIS aerosol products over land and ocean. Atmos. Meas. Tech. 6 (11), 2989.
Luo, M., Hou, X., Gu, Y., et al., 2018. Trans-boundary air pollution in a city under various atmospheric conditions. Sci. Total Environ. 618, 132–141.
Ma, Z., Liu, Y., Zhao, Q., et al., 2016a. Satellite-derived high resolution $PM_{2.5}$ concentrations in Yangtze River Delta Region of China using improved linear mixed effects model. Atmos. Environ. 133, 156–164.
Ma, Z., Hu, X., Huang, L., et al., 2014. Estimating ground-level PM2.5 in China using satellite remote sensing. Environ. Sci. Technol. 48 (13), 7436–7444.
Ma, Z., Hu, X., Sayer, A.M., et al., 2016b. Satellite-based spatiotemporal trends in PM2.5 concentrations: China, 2004–2013. Environ. Health Perspect. 124 (2), 184.
Martin, R.V., 2008. Satellite remote sensing of surface air quality. Atmos. Environ. 42 (34), 7823–7843.
Nichol, J.E., Bilal, M., 2016. Validation of MODIS 3 km resolution aerosol optical depth retrievals over Asia. Remote Sens. 8 (4), 328.
Paciorek, C.J., Liu, Y., Moreno-Macias, H., et al., 2008. Spatiotemporal associations between GOES aerosol optical depth retrievals and ground-level PM2.5. Environ. Sci. Technol. 42 (15), 5800–5806.
Qin, K., Rao, L., Xu, J., et al., 2017. Estimating ground level NO2 concentrations over central-eastern China using a satellite-based geographically and temporally weighted regression model. Rem. Sens. 9 (9), 950.
Remer, L.A., Mattoo, S., Levy, R.C., et al., 2013. MODIS 3 km aerosol product: algorithm and global perspective. Atmos. Meas. Tech. 6 (7), 1829.
Song, W., Jia, H., Huang, J., et al., 2014. A satellite-based geographically weighted regression model for regional PM2.5 estimation over the Pearl River Delta region in China. Remote Sens. Environ. 154, 1–7.
Sayer, A.M., Hsu, N.C., Bettenhausen, C., et al., 2013. Validation and uncertainty estimates for MODIS Collection 6 “Deep Blue” aerosol data. J. Geophys. Res.: Atmosphere 118 (14), 7864–7872.
Tang, L., Yu, H., Ding, A., et al., 2016. Regional contribution to PM1 pollution during winter haze in Yangtze River Delta, China. Sci. Total Environ. 541, 161–166.
Tao, M., Chen, L., Wang, Z., et al., 2015. Comparison and evaluation of the MODIS Collection 6 aerosol data in China. J. Geophys. Res.: Atmosphere 120 (14), 6992–7005.
Tao, J., Shen, Z., Zhu, C., et al., 2012. Seasonal variations and chemical characteristics of sub-micrometer particles (PM1) in Guangzhou, China. Atmos. Res. 118, 222–231.
Tian, J., Chen, D., 2010. A semi-empirical model for predicting hourly ground-level fine particulate matter (PM2.5) concentration in southern Ontario from satellite remote sensing and ground-based meteorological measurements. Remote Sens. Environ. 114 (2), 221–229.
Tong, C.H.M., Yim, S.H.L., Rothenberg, D., et al., 2018a. Assessing the impacts of seasonal and vertical atmospheric conditions on air quality over the Pearl River Delta region. Atmos. Environ. 180, 69–78.
Tong, C.H.M., Yim, S.H.L., Rothenberg, D., et al., 2018b. Assessing the impacts of seasonal and vertical atmospheric conditions on air quality over the Pearl River Delta region. Atmos. Environ. 180, 69–78.
Tong, C.H.M., Yim, S.H.L., Rothenberg, D., et al., 2018c. Projecting the impacts of atmospheric conditions under climate change on air quality over Pearl River Delta region. Atmos. Environ. 193, 79–87.
Van Donkelaar, A., Martin, R.V., Park, R.J., 2006. Estimating ground-level PM2.5 using aerosol optical depth determined from satellite remote sensing. J. Geophys. Res.: Atmosphere 111 (D21).
Van Donkelaar, A., Martin, R.V., Brauer, M., et al., 2010. Global estimates of ambient fine particulate matter concentrations from satellite-based aerosol optical depth: development and application. Environ. Health Perspect. 118 (6), 847.
Wang, J., Christopher, S.A., 2003. Intercomparison between satellite-derived aerosol optical thickness and PM2.5 mass: implications for air quality studies. Geophys. Res. Lett. 30 (21).
Wang, Z., Chen, L., Tao, J., et al., 2010. Satellite-based estimation of regional particulate matter (PM) in Beijing using vertical-and-RH correcting method. Remote Sens. Environ. 114 (1), 50–63.
Wang, T., Jiang, F., Deng, J., et al., 2012. Urban air quality and regional haze weather forecast for Yangtze River Delta region. Atmos. Environ. 58, 70–83.
Wu, Y., Guo, J., Zhang, X., et al., 2012. Synergy of satellite and ground based observations in estimation of particulate matter in eastern China. Sci. Total Environ. 433, 20–30.
World Health Organization, 2006. WHO Air Quality Guidelines for Particulate Matter, Ozone, Nitrogen Dioxide and Sulfur Dioxide-Global Update 2005-Summary of Risk Assessment, 2006. WHO, Geneva.
Xie, Y., Wang, Y., Zhang, K., et al., 2015. Daily estimation of ground-level $PM_{2.5}$ concentrations over Beijing using 3 km resolution MODIS AOD. Environ. Sci. Technol. 49 (20), 12280–12288.
Xu, H., Guo, J., Ceamanos, X., Roujean, J., Min, M., Carrer, D., 2016. On the influence of the diurnal variations of aerosol content to estimate direct aerosol radiative forcing using MODIS data. Atmos. Environ. 141, 186–196. https://doi.org/10.1016/j.atmosenv.2016.06.067. 2016.
Yang, Y., Zheng, X., Gao, Z., et al., 2018. Long-term trends of persistent synoptic circulation events in planetary boundary layer and their relationships with haze pollution in winter half-year over eastern China. J. Geophys. Res.: Atmosphere. https://doi.org/10.1029/2018JD028982.
You, W., Zang, Z., Zhang, L., et al., 2016. Estimating national-scale ground-level PM25 concentration in China using geographically weighted regression based on MODIS and MISR AOD. Environ. Sci. Pollut. Control Ser. 23 (9), 8327–8338.
Yu, W., Liu, Y., Ma, Z., et al., 2017. Improving satellite-based $PM_{2.5}$ estimates in China using Gaussian processes modeling in a Bayesian hierarchical setting. Sci. Rep. 7 (1), 7048.
Zang, L., Mao, F., Guo, J., Gong, W., Wang, W., Pan, Z., 2018. Estimating hourly PM_1 concentrations from Himawari-8 aerosol optical depth in China. Environ. Pollut. 241, 654–663. https://doi.org/10.1016/j.envpol.2018.05.100.
Zou, B., Pu, Q., Bilal, M., et al., 2016a. High-resolution satellite mapping of fine particulates based on geographically weighted regression. Geosci. Rem. Sens. Lett. IEEE 13 (4), 495–499.
Zou, B., Chen, J., Zhai, L., et al., 2016b. Satellite based mapping of ground PM2. 5 concentration using generalized additive modeling. Rem. Sens. 9 (1), 1.
Zheng, Y., Zhang, Q., Liu, Y., et al., 2016. Estimating ground-level PM2.5 concentrations over three megalopolises in China using satellite-derived aerosol optical depth measurements. Atmos. Environ. 124, 232–242.
Zhang, W., Guo, J., Miao, Y., Liu, H., Song, Y., Fang, Z., He, J., Lou, M., Yan, Y., Li, Y., Zhai, P., 2018. On the summertime planetary boundary layer with different thermodynamic stability in China: a radiosonde perspective. J. Clim. 31 (4), 1451–1465. https://doi.org/10.1175/JCLI-D-17-0231.1.